J Mater Sci (2009) 44:5636–5643
DOI 10.1007/s10853-009-3794-z

Electron spin resonance study of Mo(V) ion species incorporated into aluminosilicate nanospheres with solid core/mesoporous shell structure

Gernho Back · Hyeyoung Lee · Minsik Kim · Jong-Sung Yu · Soobok Jeong · Young Bae Chae

Received: 13 February 2009 / Accepted: 5 August 2009 / Published online: 19 August 2009

Abstract Silica spheres with sub-micrometer sized solid core and mesoporous shell (SCMS) structure were synthesized, and aluminum was incorporated into the mesoporous shell framework by impregnation method to generate SCMS aluminosilicate (AlSCMS) nanospheres. The impregnation of aluminum into the SCMS spheres generates the acid sites on the framework due to the presence of Al^{3+} ions. The AlSCMS was then used to support molybdenum ion species on the mesoporous shell framework. A solid-state reaction of MoO_3 with AlSCMS followed by thermal reduction generated paramagnetic Mo(V) species. The dehydration produced a Mo(V) species that is characterized by electron spin resonance with $g_e > g_\perp > g_{||}$. The structural properties of active sites in the AlSCMS were characterized by means of XRD, UV–Vis, ^{27}Al MAS NMR, FT-IR, and energy dispersive X-ray spectrometric measurements. Upon O_2 adsorption, the Mo(V) ESR signal intensity decreased, and a new O_2^- radical was generated. The Mo species in the dehydrated Mo-AlSCMS is found to exist as oxo-molybdenum species, $(MoO_2)^+$ or $(MoO)^{3+}$. Since the AlSCMS has a low framework negative charge, the MoO_2^+ with a low positive charge can be easily stabilized and thus seems to be more probable in the AlSCMS framework.

G. Back (✉) · H. Lee
Department of Chemistry, Changwon National University, 9 Sarim-dong, Changwon, Kyungnam 641-773, Korea
e-mail: ghbaek@changwon.ac.kr

M. Kim · J.-S. Yu (✉)
Department of Advanced Materials Chemistry, BK21 Research Team, Korea University, 208 Seochang, Jochiwon 339-700, Korea
e-mail: jsyu212@korea.ac.kr

S. Jeong · Y. B. Chae
Mineral Resource Research Division, Korea Institute of Geoscience and Mineral Resources, Gajeong-dong 30, Yusong-gu, Daejeon 305-350, Republic of Korea

Introduction

Considerable interest in nanoporous materials such as zeolites and mesoporous molecular sieves stems from application potential towards catalysis, adsorption, separation processes, drug delivery and release, and optical and electrochemical process due to their well-developed ordered porous structures with high specific surface area, large pore volume, and narrow pore size distribution [1–3]. Amine molecules or surfactant micelles have been used as structure directing templates for the fabrication of the nanoporous materials [4–8]. These porous materials were mostly produced in amorphous powder type. Recently, porous materials with specific morphologies as well as the mesostructure have attracted enormous attentions due to more specific applications [9, 10]. Thus, the synthesis of tailored nanostructured particle has been a major challenge in advanced materials science. The focus mainly lies on understanding the formation mechanism of the nanostructured particles and on the conditions to tailor their particle morphology, particle size, and pore structure [10]. Many new nanostructured shell frameworks with either solid core or hollow core were generated depending on the removal of core templates, some of which were applied to controlled materials release through nanoporous shell [9–12].

Recently, structurally important novel sub-micrometer sized silica spheres with solid core and mesoporous shell (SCMS) structure were synthesized [11]. The core size and/or shell thickness of the SCMS particles can be controlled independently by two separate synthesis processes,

consisting of solid core formation by the Stöber method (first step) and subsequent formation of the mesoporous shell by the Kaiser approach (second step) [13, 14]. Octadecyltrimethoxysilane (C_{18}-TMS) has been used as a porogen to generate the mesopores in the shell. The mesoporous silica layer on each silica particle was generated by co-hydrolysis and subsequent condensation of tetraethoxysilane and the C_{18}-TMS. The mesopores in the shell of the SCMS particles can be regulated with ordered or disordered arrangement depending on the types of pore-generating surfactants [8]. Like all the mesoporous silica materials, the silicon dioxide in the silica walls surrounding the SCMS spheres possesses an amorphous nature [1–3]. The incorporation of aluminum into the SCMS framework causes a negative net charge on the framework that is compensated by protons. Therefore, it is expected that aluminum-containing SCMS (AlSCMS) silica spheres will possess an ion-exchange capacity by other charge balancing cations such as paramagnetic transition metal ions as found in zeolite [15, 16]. Such transition metal ion species in the AlSCMS system may offer potential for specially tailored catalytic applications [17].

It is well-known that molybdenum-loaded catalysts are useful for industrial processes such as Fischer-Tropsch synthesis, epoxidation, and methanation [18]. Also, oxomolybdenum complexes catalyze a number of biologically important oxo-transfer reactions such as conversion of sulfite to sulfate and xanthine to uric acid [19]. The molybdenum species have been investigated on silica and alumina [20], Y [21], ZSM-5 [17], mordenite zeolites [22], and silicoaluminophosphate (SAPO) molecular sieves [23–25]. From those studies it was concluded that Mo(V) has various coordinations depending on the support and the preparation methods and that these determine the catalytic activity [25, 26]. However, there is only a few study about Mo species supported on mesoporous materials. MoO_3 supported on hexagonal mesoporous silica power was reported as efficient Mo catalyst for olefin metathesis [27]. Mo-MCM-41 was examined for photocatalytic reactivity [28]. Mo-containing Al-MCM-41 catalysts were also tested for thiophene hydrodesulfurization [29]. However, there has been no study about the structure and application of Mo species in mesoporous materials with structurally important morphology despite their importance in catalysis and adsorption. In particular, the potential catalytic application of the metal ion sites requires detailed characterization of their environment in the mesoporous materials including their framework position and coordination structure.

In the present work, Mo ion species were exchanged for the first time into the mesoporous framework through solid-state reaction of MoO_3 with the AlSCMS nanospheres to form Mo(VI)-AlSCMS. The paramagnetic Mo(V) species generated by thermal reduction were characterized by electron spin resonance (ESR), FT-IR, and UV–Vis spectroscopy to gain information about the coordination of the Mo species. This study illustrates that the Mo(V) ion species in dehydrated Mo-AlSCMS exists as $(MoO_2)^+$ or $(MoO)^{3+}$ in an extra-framework position.

Experiments

Synthesis of SCMS aluminosilicate spheres

Solid core and mesoporous shell silica was synthesized according to literature [11, 12], and the following procedure describes the synthesis of the SCMS silica spheres with a core diameter of 180 nm and a shell thickness of 50 nm. About 3.14 mL of aqueous ammonia (32 wt%) was added to a solution containing 74 mL of ethanol and 10 mL of deionized water. Six milliliter of tetraethoxysilane (TEOS) was added to the above-prepared mixture at 303 K with vigorous stirring and the reaction mixture was stirred continuously for 1 h to yield uniform silica spheres (Stöber silica solution). A mixture solution containing 5 mL of TEOS and 2 mL octadecyltrimethoxysilane (C_{18}-TMS) (90%, Aldrich) (i.e., molar ratio of TEOS to C_{18}-TMS = 4.7) was added to the colloidal solution containing the silica spheres and further reacted for 1 h. The resulting octadecyl group incorporated silica particles were retrieved by centrifugation, and further calcined at 823 K for 6 h under an oxygen atmosphere to produce the final SCMS silica material. Aluminum was incorporated into the silicate framework through an impregnation method. A total of 1 g of the SCMS silica was added an aqueous solution containing 0.27 g of $AlCl_3{\cdot}6H_2O$ in 0.3 mL of water, and the resulting slurry was stirred for 30 min. The powder was dried in air at 353 K. Finally, the Al-impregnated SCMS silica was calcined at 823 K for 5 h in air to yield SCMS aluminosilicate (AlSCMS).

Synthesis of Mo-AlSCMS

Mo-AlSCMS material was prepared by a procedure similar to the procedure for Mo-SAPO-34 [24]. 0.0048 g of natural MoO_3(Aldrich) was ground well in a mortar with a pestle followed by mixing with 0.2359 g of calcined AlSCMS for 30 min. The mixture was pressed in a stainless steel die with a force of 2.5 ton for 10 min to produce a pellet with 10 mm diameter × 4 mm thickness in size. The pellet was ground to a fine powder and then calcined at 828 K for 10 h in flowing oxygen. After calcinations, the as-synthesized Mo-AlSCMS was cooled to room temperature and put in a desiccator.

Sample treatment and measurements

N_2 adsorption and desorption isotherms were measured at 77 K on a KICT SPA-3000 Gas Adsorption Analyzer after the sample was degassed at 423 K to 20 μ Torr for 12 h. The specific surface areas were determined from nitrogen adsorption using the Brunauer–Emmett–Teller (BET) equation. Total pore volume was determined from the amount of gas adsorbed at the relative pressure of 0.99. Pore size distribution (PSD) was derived from the analysis of the adsorption branch using the Barrett–Joyner–Halenda (BJH) method.

Powder X-ray diffraction (XRD) patterns were recorded on a Phillips PW 1840 X-ray diffraction using Cu Kα radiation with a wavelength 1.541 Å. Chemical analysis of the samples was carried out with Oxford Energy dispersive X-ray spectrometer. The MAS-NMR spectra were recorded at 9.4 T using a Bruker DSX600 solid-state NMR spectrometer. ^{27}Al-MAS spectra were measured at 104.18 MHz using a $\pi/20$ pulse and a recycle delay time of 1 s. The 4 mm rotor was spun at a frequency of 13.2 kHz. External $AlCl_3$ was used as a chemical shift reference. Ammonia-TPD (temperature programmed desorption) was performed with gas chromatography (Micromertex Autopure 2920) attached with TCD (thermal conductive detector). The AlSCMS and SCMS samples were filled into the quartz tube and finally connected in the vacuum line on-lined with gas chromatography. The samples were activated in situ at 573 K for 3 h in the presence of high-purity helium with a flow rate of 140 mL/min to remove physically adsorbed water and then cooled to 298 K. The samples subsequently were adsorbed with NH_3 at 373 K for 2 h. NH_3-TPD was performed at the region of 373–1073 K with the heating rate 278 K/min. The diffuse reflectance (DR) UV–Vis spectra were recorded using a Varian model Cary 1C spectrometer with an integrating sphere accessory.

ESR spectra were recorded with 300 MHz spectrometer (Jeol model JES-FA) at 77 and 298 K using 3 mm o.d. × 2 mm i.d. Suprasil quartz tube. Magnetic field was calibrated with a Jeol model ES-FCB gauss meter. The as-synthesized Mo-AlSCMS was first evacuated to a final pressure of 10^{-4} Torr and then heated under vacuum from 295 to 773 K at regular intervals to study the behavior of the Mo species as a function of the dehydration. The temperature was raised slowly and held at several temperatures, each for 5–10 h. ESR spectra were measured at 77 K to observe the change of the Mo species in the Mo-AlSCMS. To study the redox behavior of the Mo species, the dehydrated sample at 773 K was contacted with 50 Torr of O_2 at RT for 2 min and then evacuated at same temperature briefly for 1 min to remove physically attached oxygen. FT-IR spectra were recorded with Nicolet Impact 410 DSP spectrometer using KBr pellets coupled to an AT-386 SX computer.

Results and discussion

Characterization of AlSCMS

Figure 1a and b show the scanning electron microscopic (SEM) and transmission electron microscopic (TEM) images of the AlSCMS. The SEM image reveals that the particles are spherical and uniform with diameters of ~280 nm and no agglomeration takes place. The TEM image shows clearly a 180 nm sized core and a 50 nm thick mesoporous shell. The mesopores were randomly distributed over the shell, whereas the core was dense and non-porous. Some particles are deformed, and this deformation seems to be the result of mechanical stress during the thermal removal of octadecyl groups incorporated in the silica particles.

XRD patterns of the AlSCMS are shown in Fig. 1c. The XRD pattern typical of hexagonal-type mesoporous structure despite being rather poorly resolved could be obtained with a d-spacing of ca. 3.3 nm. The unit cell parameter (a_0) was calculated to be 3.8 nm on the basis of $2d_{100}/\sqrt{3}$ from d_{100} which is obtained from 2θ of the first peak in the XRD pattern by Bragg's equation [30] ($2d\sin\theta = \lambda$, $\lambda = 1.541$ Å for the Cu Kα line). Chemical analysis of the AlSCMS samples was carried out with Oxford Energy dispersive X-ray spectrometer. The ratio for Si/Al is found to be 11.

Typical nitrogen sorption isotherms at 77 K and the corresponding pore size distribution are shown in Fig. 1d. The nitrogen isotherms indicate a linear increase of the amount of adsorbed nitrogen at low pressures (less than $p/p_0 = 0.25$), and a hysteresis between the adsorption branch and the desorption branch appears. The resulting isotherm can be classified as a type IV isotherm with H2-type hysteresis according to the IUPAC nomenclature. The steep increase in nitrogen uptake at relative pressures in the range between $p/p_0 = 0.3$ and 0.50 is reflected in a narrow pore size distribution. The pore size from the PSD maximum was estimated as ca. 2.4 nm with a narrow PSD. The AlSCMS exhibits specific surface area of ca. 396 m^2/g and total pore volume of ca. 0.32 cm^3/g, which are mainly attributable to the presence of the mesopores in the shell. From the unit cell parameter a_0, which is equal to one internal pore diameter plus one pore wall thickness, the wall thickness is determined to be 1.4 nm.

^{27}Al MAS NMR

^{27}Al MAS NMR spectroscopy was used to confirm the incorporation of aluminum into the framework of as-synthesized SCMS silica particles. The ^{27}Al MAS NMR spectrum of the sample in Fig. 2 gives a single sharp resonance at 56.2 ppm from Al in tetrahedral (framework)

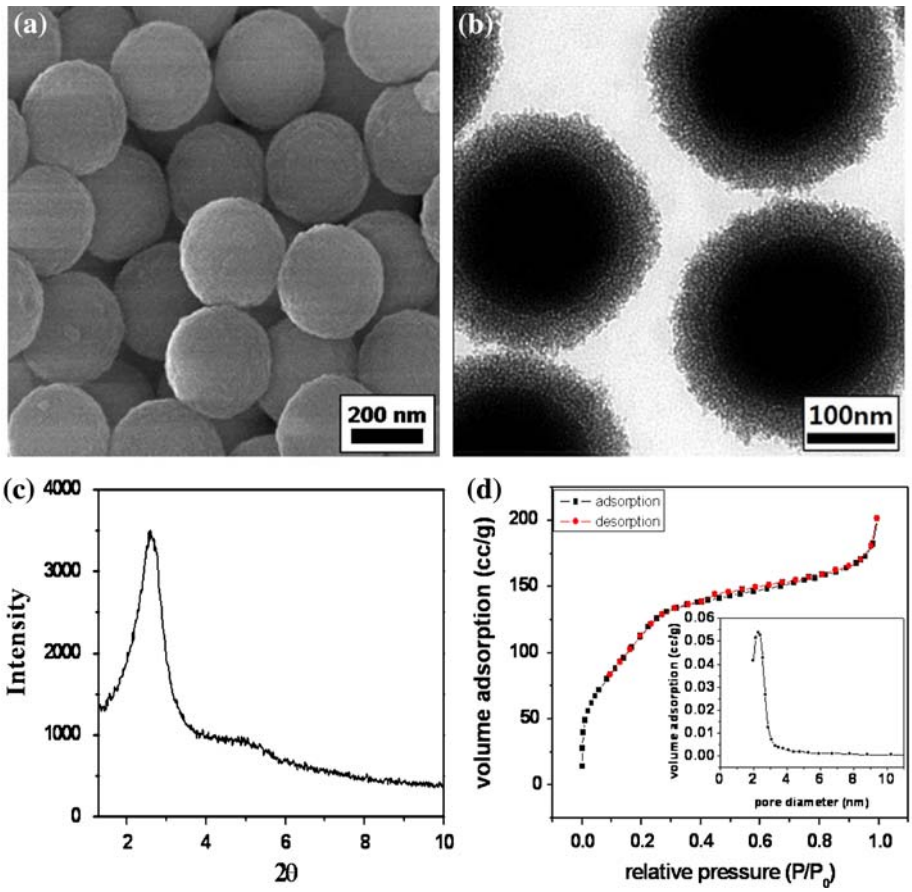

Fig. 1 **a** SEM and **b** TEM images of AlSCMS with a core diameter of 180 nm and a shell thickness of 50 nm. **c** XRD pattern of the AlSCMS. **d** Nitrogen sorption isotherms at 77 K for calcined AlSCMS and pore size distribution determined by BJH method (insert)

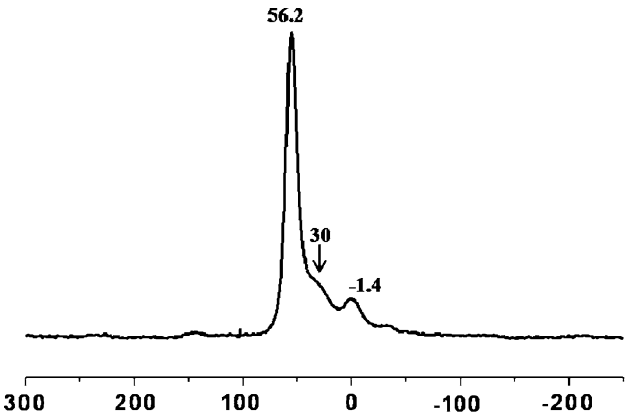

Fig. 2 ^{27}Al MAS NMR spectrum of calcined AlSCMS

coordination. In addition, less intense lines are also obtained at ca. 30 and −1.4 ppm corresponding to octahedral coordination, which indicates a non-framework Al species. A rough estimation of the intensity of the lines corresponding to the non-framework Al species compared to the intensity of the line at 56.2 ppm shows that about 70% of the Al species are framework species. The spectrum is in good agreement with the previous data [31–35], indicating it is not likely that the non-framework aluminum affects the location of Mo ion species.

Ammonia-TPD

The substitution of some silicone by aluminum in the framework of SCMS also generates acid sites in the framework. NH_3-TPD was used to confirm the acid sites. The TPD signals at 200 and 400 °C in the AlSCMS sample were 6 times and 2 times higher than those of the SCMS, respectively, as shown in Fig. 3. The comparison of the curves on Fig. 3a and b leads to a conclusion that at 400 °C AlSCMS sample has more strong acid sites than SCMS one due to the presence of framework Al of the former. The signal occurring at lower temperature of 200 °C can be assigned to non-framework Al species.

ESR investigation

To study the redox behavior of Mo-AlSCMS, as-synthesized Mo-AlSCMS was dehydrated by slowly raising the temperature from RT to 773 K. The ESR spectra of the Mo-AlSCMS samples before and after various treatments were measured and shown in Fig. 4. The as-synthesized Mo-AlSCMS before dehydration produced no ESR signal due to the diamagnetic Mo(VI) ion species. During dehydration, the Mo(VI) species is thermally reduced to the Mo species with lower oxidation state and starts to display

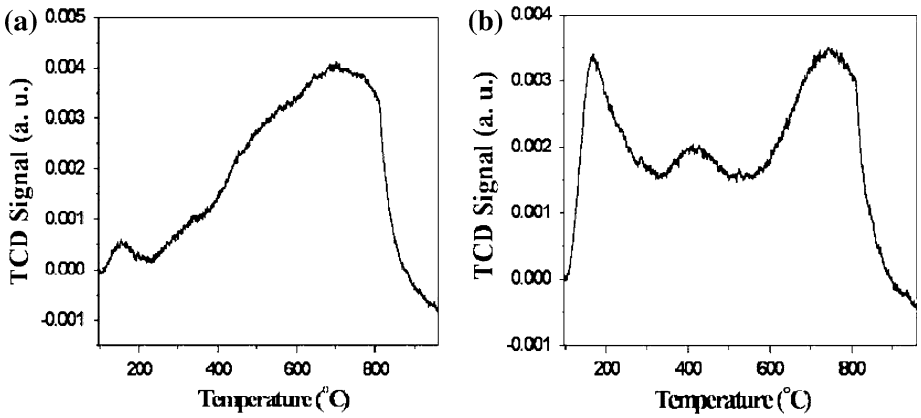

Fig. 3 Ammonia-TPD profiles for **a** SCMS and **b** AlSCMS desorbed at same heating rate of 5 °C/min

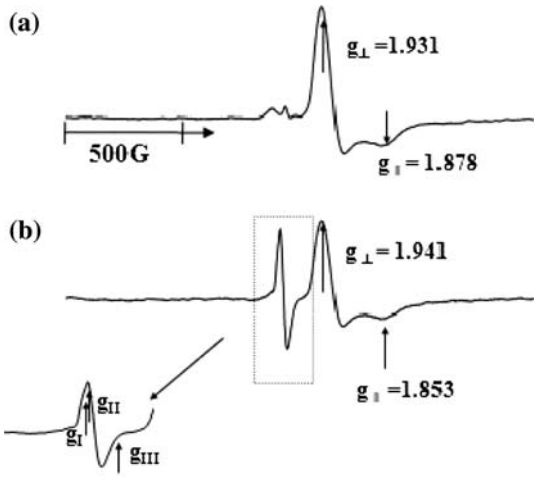

Fig. 4 ESR spectra of as-synthesized Mo-AlSCMS at 77 K **a** after dehydration at 773 K for 10 h and then **b** after 50 Torr of O_2 adsorption for 2 min at room temperature following the dehydration. The O_2^- radical signal was expanded to clearly resolve the *g* values in the bottom of **b**

axially symmetric paramagnetic ESR pattern. One main Mo species corresponding to paramagnetic Mo(V) was developed and assigned to Mo(A) with a reversed *g* value ($g_{\|} = 1.878$, $g_{\perp} = 1.931$) after dehydration at 773 K for 10 h. On the basis of previous works on Mo-SAPO-*n* systems [24, 25], two oxo-molybdenum $(MoO_2)^+$ and $(MoO)^{3+}$ are most probable for the paramagnetic Mo(A). The dioxo-molybdenum $(MoO_2)^+$ is likely coordinated to 3 framework oxygen atoms and two extra-framework oxygen atoms as $Mo(V)_{5c}$, where the subscript denoted the coordination number, while monooxo-molybdenum $(MoO)^{3+}$ is a $Mo(V)_{4c}$, coordinating to 3 framework oxygen atoms and one extra-framework oxygen atom. Since the AlSCMS possesses low framework negative charge with Si/Al ratio of 11, $(MoO)^{3+}$ with a high positive charge cannot be easily stabilized. Thus, the Mo(A) species is likely to be dioxo-molybdenum $(MoO_2)^+$ with a low positive charge existing as $Mo(V)_{5c}$ in accordance with those in SAPO system with weakly negative framework charge [24, 25, 36, 37]. The ESR parameters of the Mo species in Mo-AlSCMS sample are shown in Table 1 in comparison with the ESR parameters of previously reported Mo species in SAPO frameworks [24, 25].

Table 2 *g* values of O_2^- radicals formed in molybdenum/oxide systems

System	Species	g_1	g_2	g_3	Ref
MoO_3/SAPO-11		2.021	2.014	2.008	[25]
MoO_3/SAPO-5	(I)	2.020	2.015	2.006	[25]
	(II)[a]	2.024	2.013	2.006	[25]
MoO_3/SAPO-34	(A)[b]	2.029	2.021	2.013	[24]
	(B)[c]	2.029	2.019	2.013	[24]
MoO_3/AlSCMS		2.023	2.012	2.009	This work

[a] Produced by O_2 absorption on activated sample

[b] Major species

[c] Produced by O_2 absorption on a sample reduced by ammonia

Table 1 Comparison ESR parameters of Mo(V) in Mo-AlSCMS at 77 K along with those in MoH-SAPO-5 and 34

Treatment	Species	MoH-SAPO-5 [25]		MoH-SAPO-34 [24]		Mo-AlSCMS [this work]	
		$g_{\|}$[a]	$g_{\perp}$[a,b]	$g_{\|}$[a]	$g_{\perp}$[a,b]	$g_{\|}$[a]	$g_{\perp}$[a]
Dehydration	A	1.877	1.952	1.884	1.979	1.878	1.931
	B	1.849	1.960	1.884	1.962		

[a] Estimated uncertainty is ±0.003

[b] $g_{\perp}$ is measured at the maximum peak position of the derivative signal in order to compare with the previous literature

Upon O_2 adsorption, the Mo(V) ESR signal intensity decreases and new O_2^- radical is formed as observed previously [24, 25]. The coordinated structures can be deduced from the differences in the ESR parameters between the dehydrated species and species adsorbed with an adsorbate such as oxygen. The O_2^- radical signal was expanded for better resolution and shown in the bottom of Fig. 4b. Table 2 summarizes the ESR parameters of the O_2^- radicals formed in various molybdenum/oxide systems.

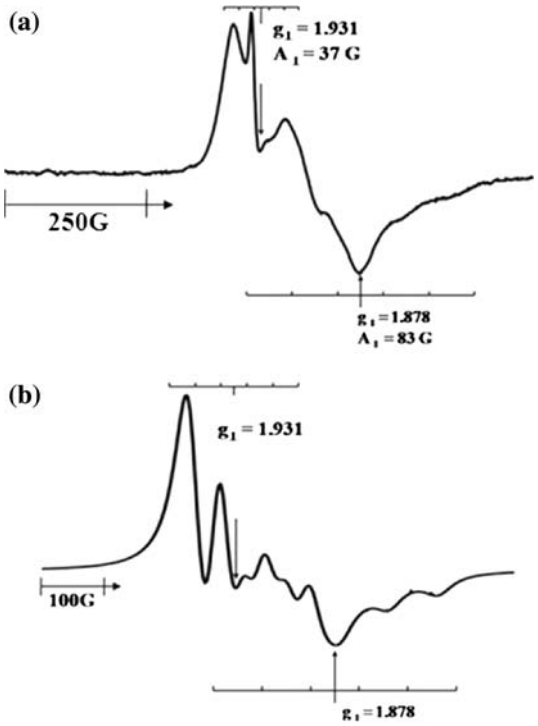

Fig. 5 **a** ESR spectrum at 77 K of dehydrated ^{97}Mo-AlSCMS at 773 K for 10 h, enriched with ^{97}Mo, and **b** simulated ESR spectrum derived with the magnetic parameters deduced from **a** spectrum

Figure 5a shows the ESR spectrum of a dehydrated ^{97}Mo-AlSCMS sample obtained with ^{97}Mo-enriched MoO_3. Interestingly, six hyperfine lines were observed with the same g values as those in Fig. 4a. The ESR parameters of ^{97}Mo-AlSCMS sample are $g_\perp = 1.931$, $A_\perp = 37$ G, and $g_{\|} = 1.878$, $A_{\|} = 83$ G. Figure 5b shows a simulated ESR spectrum revealed by EPRR (electron paramagnetic resonance running) with the magnetic parameters deduced from the spectrum in Fig. 5a. The simulated spectrum fits well the experimental one. This hyperfine was assigned to the ^{97}Mo ($I = 5/2$) isotope, which is 9.6% natural abundant.

FT-IR

The FT-IR spectrum of the Mo-AlSCMS samples is shown in Fig. 6b along with that of the reference material, AlSCMS. The Mo–O stretching bands are observed in the 950–700 cm^{-1} range, while the Al–O stretching and deformation modes are in the 600–400 cm^{-1} range [38]. An absorption peak at 673 cm^{-1} appeared after calcinations at 550 °C for 10 h of as-synthesized Mo-AlSCMS is assigned to a Mo–O band. Unfortunately, the other absorption bands near at the 946 cm^{-1} corresponding to the Mo–O stretching band could not be identified because they are expected

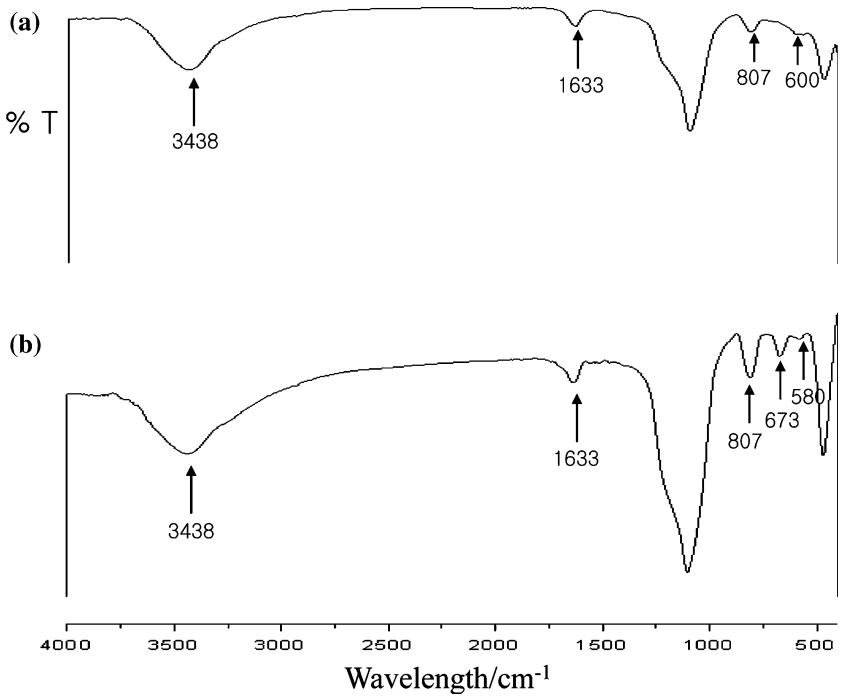

Fig. 6 FT-IR spectra of **a** reference AlSCMS and **b** Mo-AlSCMS, both of which are calcined at 550 °C for 10 h

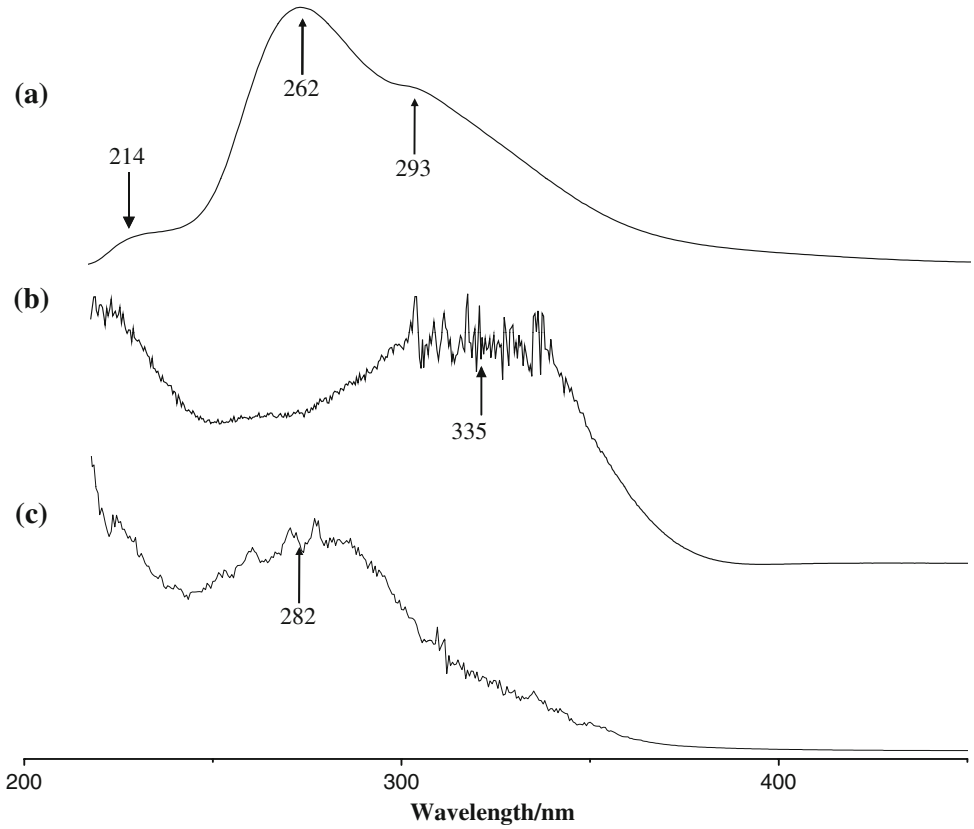

Fig. 7 Diffuse reflectance UV–Vis spectra of **a** dehydrated Mo-AlSCMS and reference materials, **b** MoO_3, and **c** $Al_2(MoO_4)_3$

to appear at absorption band similar to those of Al–O modes and silica framework [39]. It is reasonable to assign the absorption peak at 673 cm^{-1} to the asymmetrical Mo–O stretching bond.

UV–Vis investigation

DR UV–Vis spectrum of the Mo-AlSCMS sample is shown in Fig. 7a along with those of other reference molybdenum oxides. The absorption bands appeared at around 200–240 nm and 240–300 nm, which are assigned to the charge transfer from O^{2-} to Mo^{5+}, indicating that dehydrated Mo species are Mo-oxide species [24, 25, 28]. Unfortunately, the local structure of Mo oxides, such as the tetra- or penta-coordinated Mo oxide could not be clearly identified by electronic transition because they exhibit a similar energy gap between HOMO and LUMO level [28]. None of the samples showed absorption at wavelengths longer than 340 nm. The result indicates highly dispersed Mo oxides.

Conclusions

In the present work, Mo ion species was exchanged for the first time into the AlSCMS framework to form Mo(VI)-AlSCMS. Paramagnetic Mo(V) species was generated from Mo(VI) by thermal reduction during dehydration. The paramagnetic Mo(V) species were characterized by ESR, FT-IR, and UV–Vis spectroscopy to gain information about the coordination of the Mo species. The ion-exchange site seems to be located within the shell forming the mesoporous corona of the AlSCMS structure. ESR results indicate that the Mo(V) species exist as oxo-molybdenum ions as either $(MoO_2)^+$ or $(MoO)^{3+}$. The $(Mo(V)–O_2)^+$ species seems more probable due to low negative framework charge of the AlSCMS.

Acknowledgements This research was financially supported by the Changwon National University in 2007, Korea University in 2008 and KEMCO. G. Back and JSYU thank BK21program and KBSI at Daegu, Jeonju, and Daejeon for taking the ^{27}Al MAS NMR, SEM, and TEM measurements.

References

1. Beck JS, Vartuli JC, Roth WJ, Leonowicz ME, Kresge CT, Schmitt KD, Chu CT-W, Olson DH, Scheppard EW, McCullen SB, Higgins JB, Schlenker JL (1992) J Am Chem Soc 114:10834
2. Kresge CT, Leonowicz ME, Roth WJ, Vartuli JC, Beck JS (1992) Nature 359:710
3. Kang S, Chae YB, Yu J-S (2009) J NanoSci Nanotechnol 9:527
4. Yoon SB, Kim JY, Yu J-S (2002) Chem Commun 1536

5. Kim JY, Yoon SB, Kooli F, Yu J-S (2001) J Mater Chem 11:2912
6. Vinu A, Streb C, Murugesan V, Hartman M (2003) J Phys Chem B 107:8297
7. Yoon SB, Kim JY, Yu J-S (2003) Chem Commun 1740
8. Yoon SB, Kim JY, Kim JH, Park YJ, Yoon KR, Park S-K, Yu J-S (2007) J Mater Chem 17:1758
9. Kim JH, Yoon SB, Kim J-Y, Chae YB, Yu J-S (2008) Colloids Surf A: Phys Eng Aspect 313:77
10. Yu J-S, Yoon SB, Lee YJ, Yoon KB (2005) J Phys Chem B 109:7040
11. Yoon SB, Sohn K, Kim JY, Shin C-H, Yu J-S, Hyeon T (2002) Adv Mater 14:19
12. Ji Q, Acharya S, Hill JP, Vinu A, Yoon SB, Yu J-S, Sakamoto K, Ariga K (2009) Adv Funct Mater 19(11):1792–1799
13. Stöber W, Fink A, Bohn E (1968) J Colloid Interface Sci 26:62
14. Kaiser C (1996) PhD Thesis, Johannes Gutenberg-Universitat Mainz, Germany
15. Kevan L (1987) Acc Chem Res 20:1
16. Michalik J, Brown D, Yu J-S, Danilczuk M, Kim JY, Kevan L (2001) Phys Chem Chem Phys 3:1705
17. Ma D, Zhang W, Shu Y, Liu X, Xu Y, Bao X (2000) Catal Lett 66:155–160
18. Saito M, Anderson RB (1981) J Catal 67:296
19. Spencer JT (1983) Coord Chem Rev 48:59
20. Howe RF, Leith IR (1973) J Chem Soc Faraday Trans 1 69:1967
21. Abdo S, Howe RF (1983) J Phys Chem 87:1722
22. Min-Ming H, Johns JR, Howe RF (1988) J Phys Chem 92:1291
23. Huang M, Yao J, Xu S, Meng C (1992) Zeolites 12:810
24. Back G, Jang C, Ru C, Cho YH, So H, Kevan L (2002) J Korean Chem Soc 46(1):26
25. Lee CW, Saint-Pierre T, Azuma N, Kevan L (1993) J Phys Chem 97:11811
26. Louis C, Che M (1987) J Phys Chem 91:2875
27. Ookosh T, Onaka M (1998) Chem Commun 2399
28. Higashimoto S, Hu Y, Tsumura R, Iino K, Matsuoka M, Yamashita H, Shul YG, Che M, Anpo M (2005) J Catal 235(2):272
29. Kostova NG, Kraleva E, Spojakina AA, Godocikova E, Balaz P (2007) J Mater Sci 42:3321. doi:10.1007/s10853-006-0817-x
30. Cullity BD (1987) Elements of X-ray diffraction. Addison-Wesley, Reading, MA, p 87
31. Chen C-Y, Li H-X, Davis ME (1993) Microporous Mater 2:17
32. Luan Z, Cheng C-F, Zhou W, Klinowski J (1995) J Phys Chem 99:1018
33. Borade RB, Clearfield M (1995) Catal Lett 99:10019
34. Schmidt R, Akporiae D, Stöker M, Ellestad OH (1994) In: Weitkamp J, Karge HG, Pfeiffer H, Hölderlich W (eds) Zeolites and related microporous materials: state of the art 1994: studies in surface science and catalysis, vol 84. Elsevier, Amsterdam, p 61
35. Pöppl A, Hartmann M, Kevan L (1995) J Phys Chem 99:17251
36. Back GH, Yu J-S, Kurshev V, Kevan L (1994) J Chem Soc Faraday Trans 90:2283
37. Kim BY, Yu J-S, Lee CW (2000) Bull Korean Chem Soc 21(2):251
38. Carrzán SRG, Martín C, Rives V, Vidal R (1996) Spectrochima Acta A 52:1107
39. Keller RJ (1985) In: The sigma library of FT-IR spectra, 1st edn, vol 2. Sigma Chemical Co. Inc., p 1039